Parametric Sparse Representation of Target Vibrations in SAR Using Orthogonal Matching Pursuit

1st Finlay Rollo
Sensor Signal Processing and Security Labs
University of Strathclyde
Glasgow, Scotland, UK
finlay.rollo.2019@uni.strath.ac.uk

2nd Carmine Clemente
Sensor Signal Processing and Security Labs
University of Strathclyde
Glasgow, Scotland, UK
carmine.clemente@strath.ac.uk

***Abstract*—This paper proposes a method of precise micro-Doppler analysis of vibrating targets in synthetic aperture radar (SAR) imagery. The raw SAR data is first processed using a modified backprojection approach to generate a time series of the ground target before a sparse representation approach using the orthogonal matching pursuit algorithm is used to de-noise the data. By incorporating the actual pulse timings from the SAR metadata during the dictionary construction, the method effectively handles the variable pulse repetition frequencies of modern SAR sensors. Experimental validation with real spaceborne SAR data containing an oscillating corner reflector demonstrates millimeter-level displacement accuracy, confirming the efficacy of the proposed approach for precise vibration measurement.**

***Index Terms*—Synthetic Aperture Radar, micro-Doppler, Vibration, Orthogonal Matching Pursuit, Sparse Representation**

I. Introduction

Synthetic Aperture Radar (SAR) is a remote sensing technology that uses back-scattered radar signals to create high-resolution images. SAR operates in the microwave spectrum, which unlike optical sensors, allows it to capture images regardless of weather or lighting conditions. SAR achieves a high along-track resolution using the motion of the radar platform, such as an aircraft or satellite, to synthesize a long virtual antenna, with the high cross-range resolution being dependent on the high bandwidth of the transmitted pulses.

There is an ever-increasing availability of such high-resolution, spaceborne SAR images and this opens the door for new methods of exploiting SAR imagery. Among these is the analysis of the micro-Doppler effect.

Micro-Doppler analysis extends the classical Doppler effect by accounting for time-varying frequency modulations induced by target micro-motions, such as vibrations, rotations, or oscillations [1]. Sources of such micro-motion can range from anything from the rotating blades of a helicopter or wind turbine all the way down to the swinging arms and legs of a person walking. Specifically for SAR there is significant interest in this field with a multitude of example use cases such as enhanced target characterization [2], structural health monitoring [3] and maritime domain awareness [4].

Some previous techniques utilizing the target's phase history have been proposed with some success. The authors in [5] and [6] used various forms of time-frequency analysis, such as the short-time Fourier transform and the Wigner-Ville distribution to characterize the vibrational periods of targets. While these techniques can be accurate, they require interpretation of the time-frequency distributions. An algorithm that returns a numerical solution was detailed in [7], which uses the discrete fractional Fourier transform to estimate target accelerations in a sliding window across the phase history. A similar approach that used the high-order ambiguity function was proposed in [8] with application to infrastructure monitoring.

In this paper, an approach to characterize target vibrations using SAR is proposed which makes use of a modified backprojection algorithm (BPA) and parametric sparse representation. The modified BPA is an adapted focusing procedure that is used here to generate the signal of interest that contains the target vibration information. This signal is then processed using a parametric sparse representation method, using the orthogonal matching pursuit (OMP) [9], to reduce noise and enhance the extracted features. Both sparse and parametric sparse representation techniques have previously been used for improving micro-Doppler signature classification with real aperture radars, as seen in [10]–[12]. However, to the best of the authors knowledge, this is the first instance of these techniques being used for micro-Doppler analysis in SAR.

A parametric sparse representation technique has been chosen here for two main reasons. First, it can work around some limitations, such as the restricted isometry property, typically required in standard compressed sensing frameworks. Secondly, by utilizing domain knowledge in the construction of the parametric dictionary, it can more effectively capture the key features of the underlying signal. This results in improved reconstruction accuracy and robustness to noise.

The remainder of the paper is organized as follows: Section II introduces the modified BPA approach as well as the signal model used in the sparse representation, Section III-A describes parametric sparse representation as well as the OMP algorithm. Section IV shows the results on real experimental

SAR data with sections V and VI providing the discussion and conclusion to this paper.

II. Background

A. Modified Backprojection Algorithm

The modified backprojection algorithm was recently introduced as an accurate way to extract micro-motion extraction information from SAR [13]. This has been verified on simulated data and on real spaceborne SAR data.

To briefly summarize the modification, the structure of the standard BPA remains intact, with only the coherent summation step being changed. Instead it is replaced by a concatenation, which changes the output from a 2D image to a 3D data cube where the new third dimension corresponds to time. By selecting an appropriate target pixel, details of the target's movement can be inferred from changes in the complex value of the pixel.

The key advantage of using the modified BPA to generate the signal of interest this way is its ability to achieve localized micro-Doppler extraction in both time and space while preserving image formation capabilities - full image formation can be accomplished by simply summing along the third dimension. The limitation of this approach is the significant memory required to store the resulting data cube. This could be mitigated by leveraging any a priori target information to create only the necessary image size and by selectively using pulses that correspond to moments when the target exhibits micro-motions. The computational time also remains comparable to that of the standard BPA.

B. Micro-Doppler Signal Model

The (real aperture) radar echoes from a steady-state, constant-frequency vibrating target can be modeled as a sinusoidally frequency-modulated signal [1] (Chapter 2, Eq. (2.75)):

$$s_R(t) = \rho \exp\left\{ j\frac{4\pi}{\lambda} R_0 \right\} \exp\left\{ j(2\pi f t + B\sin\omega_{\mathrm{v}} t) \right\} \quad (1)$$

where ρ is the complex reflectivity of the target, λ is the carrier wavelength, R_0 is the distance from the target to the radar, f is the carrier frequency, B is a coefficient incorporating vibration displacement and the azimuth and elevation angles between the radar and target, t is slow-time and ω_{v} is the angular vibration frequency.

This model can be adapted for the returned signal of interest from the modified BPA as in Eq. (2). The assumptions being that the spatial resolution of the SAR image is sufficiently high so that the target completely occupies the resolution cell or is otherwise the dominant scatterer.

$$y(t) = \rho(t) * exp(ja_{mD} sin(\phi_{mD} + 2\pi f_{mD} t)) \quad (2)$$

Here, $\rho(t)$ now varies over time to account for the more pronounced time-varying nature of the backscattered signal in a SAR system. The parameter a_{mD} is the amplitude of the sinusoidal frequency modulation due to the target vibration (encompassing vibration displacement, carrier wavelength and elevation-angle dependence), ϕ_{mD} is an initial phase stemming from any instantaneous displacement of the vibrating target, and f_{mD} is the vibration frequency of the target. Finally, the parameter, t corresponds to the pulse repetition frequency (PRF) sampling - also know as slow-time - in the SAR acquisition.

III. Method

A. Parametric Sparse Representation

The Orthogonal Matching Pursuit (OMP) algorithm is one of many methods originating from the field of compressed sensing. Although often used to recover signals from a limited number of measurements - sometimes even surpassing the Nyquist limit [14] by exploiting signal sparsity - OMP and related algorithms are also useful for sparse representation. In sparse representation, the goal is to represent a measurement vector $\mathbf{y} \in \mathbb{C}^m$ using only a small subset of columns from an overcomplete dictionary $\mathbf{\Phi} \in \mathbb{C}^{m \times n}$, where $m \ll n$.

Specifically, we seek a sparse coefficient vector $\mathbf{x} \in \mathbb{C}^n$ satisfying

$$\mathbf{y} \approx \mathbf{\Phi}\,\mathbf{x} + \mathbf{e}, \quad (3)$$

where $\mathbf{e}$ is a noise vector and $\mathbf{x}$ contains only a small number of non-zero elements. Formally, we can write

$$\hat{\mathbf{x}} = \arg\min_{\mathbf{x}} \|\mathbf{x}\|_0 \quad \text{s.t.} \quad \|\mathbf{y} - \mathbf{\Phi}\,\mathbf{x}\|_2^2 \leq \epsilon, \quad (4)$$

with $\|\cdot\|_0$ and $\|\cdot\|_2$ denoting the ℓ_0- and ℓ_2-norms, respectively, and ϵ a chosen error threshold. Because exact ℓ_0-minimization is an NP-hard problem, greedy algorithms such as OMP [9] iteratively select dictionary columns most correlated with the current residual, refining the solution at each step.

Parametric sparse representation extends this idea by building a dictionary $\mathbf{\Phi}$ that depends on domain-specific parameters of the signal. In this work, we discretize the micro-Doppler frequency, phase, and amplitude of the model in Eq. (2) into $P \times Q \times R$ values. These parameter sets are denoted as follows:

$$f_{\mathrm{mD}} \in \left\{ f_{\mathrm{mD}_1}, \ldots, f_{\mathrm{mD}_p}, \ldots, f_{\mathrm{mD}_P} \right\}, \quad (5)$$

$$\phi_{\mathrm{mD}} \in \left\{ \phi_{\mathrm{mD}_1}, \ldots, \phi_{\mathrm{mD}_q}, \ldots, \phi_{\mathrm{mD}_Q} \right\}, \quad (6)$$

$$a_{\mathrm{mD}} \in \left\{ a_{\mathrm{mD}_1}, \ldots, a_{\mathrm{mD}_r}, \ldots, a_{\mathrm{mD}_R} \right\}. \quad (7)$$

Here, p indexes the micro-Doppler frequency values, q indexes the phase values, and r indexes the amplitude values. Each triplet $\left(f_{\mathrm{mD}_p}, \phi_{\mathrm{mD}_q}, a_{\mathrm{mD}_r} \right)$ thus corresponds to one column (atom) in the resulting parametric dictionary which captures a range of possible micro-Doppler parameters. Thus the dictionary will contain $P \times Q \times R$ or n columns. The OMP algorithm then attempts to pick only those columns most relevant to reconstructing the measurement vector $\mathbf{y}$.

The OMP algorithm itself was chosen due to its computational speed, more advanced sparse solvers should theoretically converge on the same sparse solution but with higher computational load. As such their analysis is left open to future work.

B. Application to Real Data With Variable PRF

One of the advantages of using parametric sparse representation is that when building the dictionary the timings of a variable PRF can be naturally built into each entry. A variable PRF in SAR optimizes imaging performance by reducing range and Doppler ambiguities and adapting to different observation geometries. If we were to assume a linearly spaced t we would build an ill fitting dictionary and so below details how the actual PRF is obtained.

The raw SAR data was provided in the compensated phase history data (CPHD) format. The CPHD file contains the data for each received radar pulse in the acquisition, metadata for each individual pulse and metadata for the acquisition as a whole. Among the per pulse metadata is the transmission and receive time of each pulse given as a vector. More specifically they are the 'transmit time for the center of the transmitted pulse relative to the transmit platform collection start time' and the 'receive time for the center of the echo from the scene reference point relative to the transmit platform collection start time' [15]. The difference between adjacent elements of the transmit vector corresponds to the pulse repetition interval (PRI), and we can take the reciprocal of the PRI to get the instantaneous PRF as a function of pulse number. With this process the variable nature of the PRF is highlighted, as shown in Fig. 1.

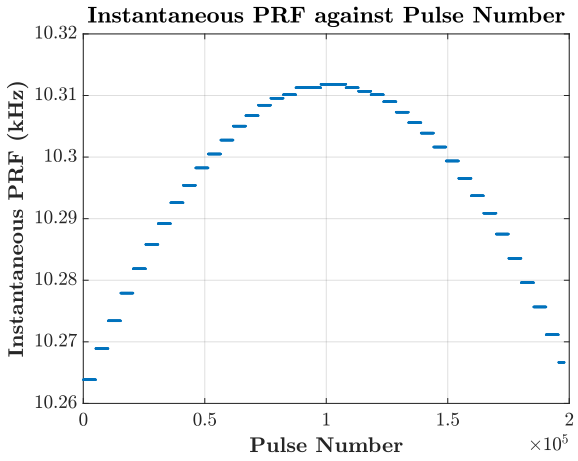

Fig. 1: Visualization of instantaneous PRF against pulse number

We can then utilize the transmit and receive times from the metadata to more accurately construct the dictionary. The time the pulse interacted with the ground, denoted t_{ground}, can be found by:

$$t_{\text{ground}} = t_{\text{transmit}} + \frac{t_{\text{receive}} - t_{\text{transmit}}}{2} \tag{8}$$

t_{ground} can then be used in place of t during dictionary construction. Finally, to further improve numerical stability, we normalize the measurement signal as:

$$y(t) = \frac{y(t)}{\max |y(t)|} \tag{9}$$

This helps to mitigate scaling discrepancies during parameter estimation, leading to a more robust sparse recovery process. Each column of the dictionary already has the unit norm, which ensures that the atom-selection step in OMP reflects correlation rather than amplitude differences across columns.

IV. Experimental Results on Real Data

This section details the experimental results obtained using real data acquired by Capella Space over Trento, Italy in December 2023. During the acquisition, a corner reflector was placed in an open field on a platform whose oscillation was controlled by a signal generator and linear servo. Synchronous ground truth was obtained using a linear variable differential transformer (LVDT) to measure the real-time displacement of the corner reflector. The platform was set to oscillate at 2 Hz with a displacement amplitude of 15 mm. Figure 2 shows the corner reflector as well as the corresponding section of the SAR image.

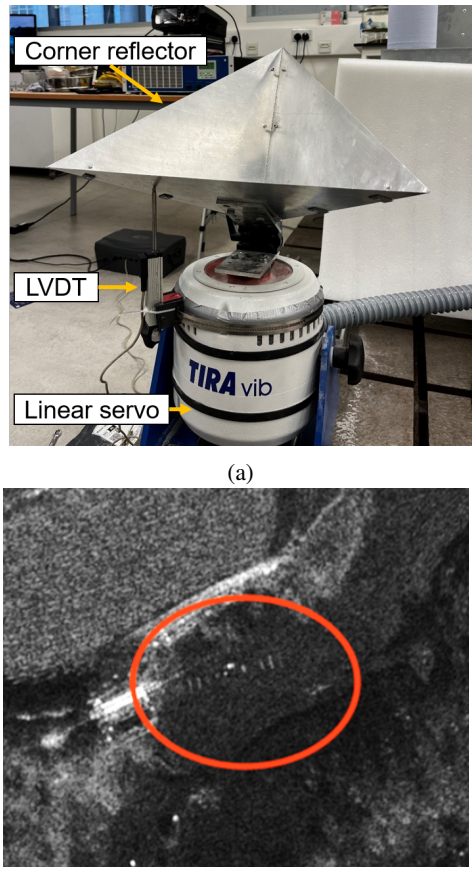

(a)

Fig. 2: (a) The apparatus used for experiments. (b) SAR image section showing the oscillating corner reflector. Image courtesy of Capella Space.

A. Time-Frequency Comparison

The micro-Doppler parameter space was discretized as follows, with candidate values taking the range:

$$f_{mD} = \{0.1, 0.2, 0.3, \ldots, 3\}, \tag{10}$$

$$\phi_{mD} = \left\{0, \frac{1\pi}{20}, \frac{2\pi}{20}, \ldots, \frac{19\pi}{20}\right\}, \tag{11}$$

$$a_{mD} = \{0.1, 0.2, 0.3, \ldots, 7\} \tag{12}$$

To ensure that the measurement vector is sufficiently smaller than the dictionary length n, not all the samples returned from the modified BPA are used. The samples are also first summed in 'batches' of 50 to increase the signal-to-noise ratio (SNR) [13]. As a result, the final measurement vector has length $m = 400$, thus satisfying the requirement $m \ll n$. Applying the OMP algorithm, the returned residual from the dictionary is sufficiently close after only one iteration, returning the parameters $f_{mD} = 2$, $a_{mD} = 5.1$, and $\phi_{mD} = \frac{9\pi}{10}$.

Taking advantage of our prior knowledge, we can use these micro-Doppler parameters to generate a denoised signal for the full duration of the aperture. It is worth noting that this is not a significantly limiting factor of this approach: if there is no a priori knowledge the OMP could simply be applied on a non-overlapping sliding window through the signal of interest though this would increase the run time.

To give a good visual understanding of the output of this process, a spectrogram of the uniformly resampled signal returned from the modified BPA has been shown alongside the reconstructed signal using parameters returned from the OMP (this uses the same sample spacing as the resampled signal) in Fig. 3.

B. Displacement Analysis

To further validate the micro-Doppler characterization, we compare the phase of the sparsely represented signal to the ground-truth measurements recorded by the LVDT. Following the approach in [13], the unwrapped, instantaneous phase of the sparsely represented signal can be related to the line-of-sight (LOS) displacement, d_{LOS}, using the wavelength λ of the center frequency of the SAR pulses. Specifically,

$$d = \frac{\Delta\phi\,\lambda}{4\pi} \tag{13}$$

where $\Delta\phi$ is the instantaneous phase.

Applying (13) to each time sample reconstructs a time series of the LOS displacement for the target pixel of interest. To compare fairly with the ground truth, we project this LOS displacement into the vertical plane via:

$$d_{\text{vertical}} = \frac{d_{\text{LOS}}}{\sin(\gamma)}, \tag{14}$$

where d_{vertical} is the vertical displacement, d_{LOS} is the line-of-sight displacement, and γ is the grazing angle of the SAR acquisition.

Figure 4 compares the reconstructed displacement using OMP with the LVDT measurements. Although the LVDT

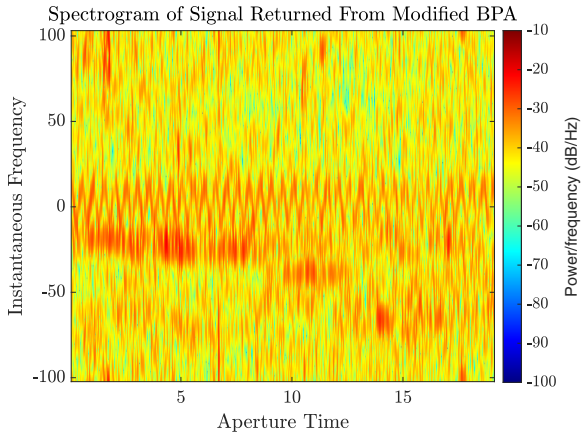

(a)

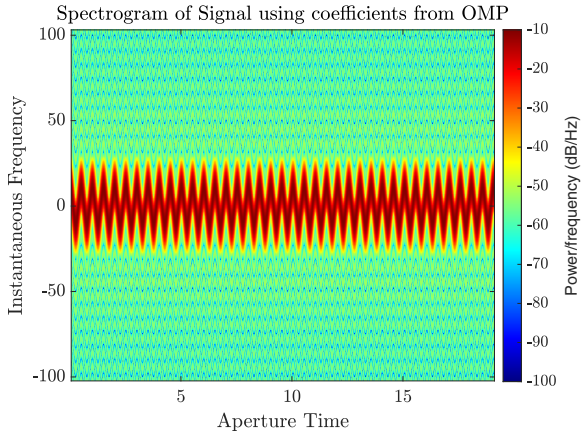

(b)

Fig. 3: (a) Spectrogram of resampled signal returned from backprojection algorithm (b) Spectrogram of signal generated using parameters returned from the OMP.

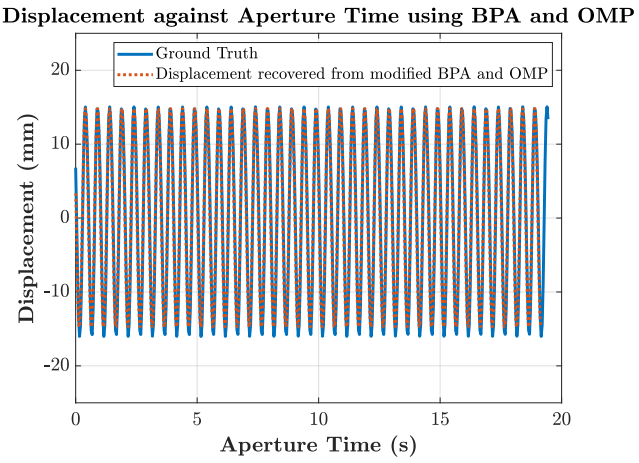

Fig. 4: Comparison of the OMP recovered signal and the ground-truth LVDT measurements.

signal is not perfectly sinusoidal - likely due to small mechanical inconsistencies in the oscillating platform - the sinusoidal model in (2) still provides more than sufficient accuracy for target characterization.

The overall displacement error remains very small, with the maximum error of any time instant being 1.27 mm (8.6%) and the mean absolute error being 0.0013 mm. This outcome is a testament to the high-quality data provided, as well as the precision in the processing needed for this level of accuracy. Of course, this result benefits from the fact that the corner reflector used provides a very strong back-scatter. If higher fidelity were required in future, the signal model could be refined to better capture non-ideal oscillations or other motion artifacts.

V. Discussion

Although the proposed approach demonstrates very promising results for vibration analysis in SAR, several avenues exist for further investigation. Firstly, additional trials will be conducted as part of our larger acquisition campaign to validate the robustness of this method under different conditions, sensor platforms, and target types. While the current experiments benefited from prior knowledge of the target's approximate vibration parameters, it would be useful to apply this approach in scenarios where such knowledge is limited or by doing blind trials.

Another natural extension of this work would be to expand the single sinusoid model to accommodate multi-component signals. This would allow for analysis of multiple vibrational modes or more complex target dynamics which is of particular interest for real world targets, such as idling vehicles or vessels. By incorporating a more flexible dictionary design or by requiring multiple iterations of the OMP, the method could capture multiple frequencies and amplitudes to better match non-ideal or multi-mode oscillations. In fact, this capability underpinned the choice of OMP over a conventional least-squares fit in this work.

A final comment is that of the ability to incorporate the precise pulse timings from the SAR metadata. This was crucial in handling the non-uniform pulse repetition frequencies. Although a uniform re-sampling strategy is sufficient for visualization in many cases, significant gaps between pulses would introduce clipping effects that compromise accuracy. Directly incorporating the true pulse timing into the dictionary construction avoids this issue and allows for accurate micro-Doppler extraction.

VI. Conclusion

This paper proposed a parametric sparse representation approach for analyzing target vibrations in SAR imagery. By first applying a modified backprojection algorithm to generate a time-domain signal, and then using the orthogonal matching pursuit algorithm, the method accurately estimated vibrational displacements even under variable pulse repetition frequencies. Experimental validation on real spaceborne SAR data demonstrated millimeter-level accuracy compared to ground-truth LVDT measurements. The approach's flexibility in dictionary construction, especially incorporating actual pulse timings, makes it well-suited to modern SAR systems. Future extensions include accommodating multi-component vibrations and investigating further optimizations for large-scale data.

Acknowledgment

Thank you to Capella Space for providing the SAR data used in this paper.
This work was supported by funding from Dstl.

References

[1] V. Chen, *The Micro-Doppler Effect in Radar*, second edition ed., 2019.

[2] C. Clemente, D. Tonelli, A. Lotti, F. Rollo, C. Ilioudis, S. D. Riofrio, F. Biondi, E. Tubaldi, M. Macdonald, D. Zonta, M. Zavagli, M. Costantini, F. Minati, F. Vecchioli, P. Milillo, M. Zimmermanns, E. Imbembo, and M. Corvino, "On micro-motion extraction from high resolution x-band sar products," in *IGARSS 2024 - 2024 IEEE International Geoscience and Remote Sensing Symposium*, 2024, pp. 1182–1186.

[3] F. Biondi, P. Addabbo, S. L. Ullo, C. Clemente, and D. Orlando, "Perspectives on the structural health monitoring of bridges by synthetic aperture radar," *Remote Sensing*, vol. 12, 2020. [Online]. Available: https://www.mdpi.com/2072-4292/12/23/3852

[4] D. Armenise, F. Biondi, P. Addabbo, C. Clemente, and D. Orlando, "Marine targets recognition through micro-motion estimation from sar data," in *2020 IEEE 7th International Workshop on Metrology for AeroSpace (MetroAeroSpace)*, 2020, pp. 37–42.

[5] V. C. Chen, F. Li, S.-S. Ho, and H. Wechsler, "Micro-doppler effect in radar: phenomenon, model, and simulation study," *IEEE Transactions on Aerospace and Electronic Systems*, vol. 42, pp. 2–21, 2006.

[6] M. Ruegg, E. Meier, and D. Nuesch, "Vibration and rotation in millimeter-wave sar," *IEEE Transactions on Geoscience and Remote Sensing*, vol. 45, pp. 293–304, 2007.

[7] Q. Wang, M. Pepin, R. J. Beach, R. Dunkel, T. Atwood, B. Santhanam, W. Gerstle, A. W. Doerry, and M. M. Hayat, "Sar-based vibration estimation using the discrete fractional fourier transform," *IEEE Transactions on Geoscience and Remote Sensing*, vol. 50, pp. 4145–4156, 2012.

[8] A. Anghel, G. Vasile, C. Ioana, R. Cacoveanu, and S. Ciochina, "Micro-doppler reconstruction in spaceborne sar images using azimuth time–frequency tracking of the phase history," *IEEE Geoscience and Remote Sensing Letters*, vol. 13, pp. 604–608, 2016.

[9] J. A. Tropp and A. C. Gilbert, "Signal recovery from random measurements via orthogonal matching pursuit," *IEEE Transactions on Information Theory*, vol. 53, no. 12, pp. 4655–4666, 2007.

[10] G. Li, R. Zhang, M. Ritchie, and H. Griffiths, "Sparsity-driven micro-doppler feature extraction for dynamic hand gesture recognition," *IEEE Transactions on Aerospace and Electronic Systems*, vol. 54, no. 2, pp. 655–665, 2018.

[11] G. Lu and Y. Bu, "Mini-uav movement classification based on sparse decomposition of micro-doppler signature," *IEEE Geoscience and Remote Sensing Letters*, vol. 21, pp. 1–5, 2024.

[12] Y. Zhao and Y. Su, "Sparse recovery on intrinsic mode functions for the micro-doppler parameters estimation of small uavs," *IEEE Transactions on Geoscience and Remote Sensing*, vol. 57, no. 9, pp. 7182–7193, 2019.

[13] F. Rollo, C. Ilioudis, G. Zefi, A. Lotti, D. Tonelli, M. Zavagli, M. Constantini, D. Zonta, E. Tubaldi, P. Milillo, M. Macdonald, and C. Clemente, "Micro-motion extraction from spotlight SAR using a modified backprojection approach," in *Microwave Remote Sensing: Data Processing and Applications III*, vol. 13195. SPIE, 2024, p. 131950D. [Online]. Available: https://doi.org/10.1117/12.3031678

[14] E. J. Candès, J. K. Romberg, and T. Tao, "Stable signal recovery from incomplete and inaccurate measurements," *Communications on Pure and Applied Mathematics*, vol. 59, no. 8, pp. 1207–1223, 2006. [Online]. Available: https://onlinelibrary.wiley.com/doi/abs/10.1002/cpa.20124

[15] "Compensated Phase History Data (CPHD) Design & Implementation Description Document," May 2018. [Online]. Available: https://nsgreg.nga.mil/doc/view?i=4638